

# Details of the mass–temperature relation for clusters of galaxies

Alexis Finoguenov, Thomas H. Reiprich and Hans Böhringer

Max-Planck-Institut für extraterrestrische Physik, Giessenbachstraße, 85748 Garching, Germany

Received October 9, 2000; accepted: December 20, 2000

**Abstract.** We present results on the total mass and temperature determination using two samples of clusters of galaxies. One sample is constructed with emphasis on the completeness of the sample, while the advantage of the other is the use of the temperature profiles, derived with ASCA. We obtain remarkably similar fits to the  $M - T$  relation for both samples, with the normalization and the slope significantly different from both prediction of self-similar collapse and hydrodynamical simulations. We discuss the origin of these discrepancies and also combine the X-ray mass with velocity dispersion measurements to provide a comparison with high-resolution dark matter simulations. Finally, we discuss the importance of a cluster formation epoch in the observed  $M - T$  relation.

**Key words:** galaxies:clusters: general – cosmology: observations; dark matter; large-scale structure of Universe

## 1. Introduction

There is increasing interest in using galaxy clusters characterized by X-ray observations as probes for cosmic structure and its evolution. In one of the applications, Press-Schechter models (Press & Schechter 1974) are used to constrain the shape and amplitude of the primordial density fluctuation spectrum at present day scales of  $5 - 10h^{-1}$  Mpc (*e.g.* Henry & Arnaud 1991, Oukbir & Blanchard 1992, Henry et al. 1992, Eke et al. 1996, 1998, Borgani et al. 1999). Another important measurement is that of the spatial correlations of X-ray clusters or, alternatively, the measurement of the power spectrum of the density fluctuations in the cluster density distribution (*e.g.* Nichol et al. 1992, Romer et al. 1994, Retzlaff et al. 1998, Miller & Batuski 2000, Schuecker et al. 2000, Collins et al. 2000). In both cases, the masses of the clusters have to be known for a large test sample in order to apply it to the structure analysis. The mass determination is still only feasible for a limited number of well-observed galaxy clusters, however. Therefore, in the above approaches the empirically-found correlation of the mass with the more easily observable parameters, X-ray luminosity or intra-

cluster gas temperature, are used to make the connection between theoretical modeling and observations. The mass-temperature relation plays a crucial role in this analysis, since it was found to be particularly tight. Since the time of the first X-ray temperature measurements it was observed that the X-ray temperature is closely connected to the velocity dispersion of galaxies in clusters, indicating that both cluster components trace the cluster potential in a similar way (*e.g.* Mushotzky et al. 1978, Mushotzky 1984).

The validity of this approach was investigated in numerical calculations based on  $N$ -body dynamic and hydrodynamic simulations making predictions on the mass-temperature relation and its dispersion, as measured in X-ray studies (Evrard, Metzler, Navarro 1996, Evrard 1997). A close correlation with a dependence of  $M \propto T^{3/2}$  was predicted. It was found in this work and also by *e.g.* Schindler (1996) that the X-ray mass determination should be reliable (with an uncertainty in the range 14 – 29%). Evrard et al. (1996 and Evrard 1997) argue, however, that the predicted mass-temperature relation has such a small dispersion that a mass estimate based on the temperature measurement only is more accurate than that determined on the basis of the additional knowledge of the gas density profile as obtained from  $\beta$ -model surface brightness profile fits. These predictions from simulations have been tested recently by means of observational results by several authors (*e.g.* Böhringer 1995, Hjorth et al. 1998, Horner et al. 1999, Nevalainen et al. 2000). Disagreements have been found concerning the predicted slope (see *e.g.* Horner et al. 1999, Nevalainen et al. 2000) and the normalization of the mass-temperature relation.

At the time of writing, this discrepancy has not been solved, and various aspects of the data analysis and simulations have been discussed: the correct measurement of temperature gradients in the intracluster gas (*e.g.* Markevitch et al. 1998; Irwin, Bregman, Evrard 1999, White 2000), influence of cooling flows (Allen 1998), non-thermal pressure support (*e.g.* Schindler 1996; Fukazawa et al. 2000), influence of the heating of the intracluster medium by supernovae (*e.g.* Balogh, Babul, Patton 1999; Loewenstein 2000; Finoguenov, Arnaud &

David 2000, hereafter FAD), density and velocity bias in the galactic component of the cluster (Colín et al. 1999) and effects of numerical resolution in the simulations (Nevalainen et al. 2000).

In this paper we reinvestigate the observational mass-temperature relation using an extended sample of clusters with measured temperature profiles covering a wide range of systems with luminosity-averaged temperatures from below 1 up to 10 keV. In particular, we include 22 low temperature systems, thus improving on sampling the low-mass part of the  $M - T$  relation, compared to previous studies (e.g. Horner et al. 1999; Nevalainen et al. 2000). To study in detail the parameters that influence the normalization and the slope of the  $M - T$  relation, we rederive the  $M - T$  relation assuming an isothermal temperature distribution and also compare with the  $M - T$  relation for *HIFLUGCS*, a statistically complete sample of clusters, described in more detail below, where the isothermality assumption was the only choice. This sample is included in our study primarily to demonstrate that the result of the  $M - T$  relation is not affected by any selection bias. In addition, we discuss implications from the results of the  $M - T$  relation study on the epoch (redshift) of cluster formation.

The paper is organized as follows. In section 2 we describe the sample compilation, in 3 we compare the results obtained for the two different samples, in 4 we combine the X-ray mass with velocity dispersion measurements to provide a comparison with high-resolution dark matter simulations and in 5 we discuss a correction for the redshift of cluster formation. Unless noted otherwise, we assume  $\Omega_M = 1$ ,  $\Lambda = 0$  and  $H_o = 50 \text{ km s}^{-1} \text{ Mpc}^{-1}$ ,  $\rho_{\text{crit,o}} = 4.6975 \times 10^{-30} \text{ g cm}^{-3}$  throughout the paper.

## 2. Data Compilation and Results

In this paper we compare the  $M - T$  relation of two cluster samples. The first is a statistically complete sample of the X-ray brightest clusters, the Highest X-ray FLUX Galaxy Cluster Sample (*HIFLUGCS*), for which the selection criteria and thus possible bias effects are well defined. For this sample, masses have been determined on the assumption of isothermality of the X-ray emitting plasma. The second sample comprises those clusters for which we have temperature profiles from ASCA observations and for which a refined mass determination is possible. For the analysis of both samples, we use the same definition of the “total mass” as the mass enclosed by the radius,  $r_{500}$ , inside which the mean cluster mass density is 500 times higher than the critical density of the Universe. Accounting for the observed redshift means that the critical density, used to calculate the overdensity, is scaled for every cluster according to its redshift. Later, in fitting the  $M - T$  relation, we correct the temperature of the cluster by dividing by  $(1 + z)$ . These corrections mean that clusters form at different epochs at similar overdensity,

so  $M3/(4\pi R^3) = 180\rho_{\text{crit,o}}(1 + z)^3$ . Therefore, for a fixed mass  $R \propto (1 + z)^{-1}$ , and  $T \propto M/R \propto (1 + z)$ . This is strictly correct only for  $\Omega_M = 1$ . However, correction for the observed redshift assuming lower values of  $\Omega_M$  has even smaller effect on the derived parameters of the  $M - T$  relation, so our correction, assuming  $\Omega_M = 1$ , can be considered as an extreme case. As we will show below, even in this case, there is no difference in the results obtained for both cluster samples considered here and thus no difference in the derived parameters of the  $M - T$  relation is expected for any value of  $\Omega_M$ .

### 2.1. HIFLUGCS

Candidates for *HIFLUGCS* have been selected from recent cluster catalogs based on the ROSAT All-Sky Survey. They have been reanalyzed homogeneously to construct a complete X-ray flux-limited sample of the brightest clusters in the sky, comprising 63 clusters. Details of the sample construction are described in Reiprich et al. (2001). The cluster masses have been calculated by assuming hydrostatic equilibrium and isothermality of the intracluster gas and determining the gas density profile with the  $\beta$  model (Cavaliere and Fusco-Femiano 1976, Gorenstein et al. 1978, Jones and Forman 1984). Overall cluster temperatures have been compiled from the literature, giving preference to temperatures measured with the ASCA satellite. The cluster masses,  $M_{500}$  and the mass errors, determined by adding the temperature error and the errors of the fit parameter values ( $\beta$  and core radius), are tabulated in Reiprich et al. (2001). Since *HIFLUGCS* is purely flux-limited, we avoid any bias that could be introduced in a subjectively compiled sample, e.g. based on the most preferred targets selected for deep observations. To maintain the completeness of the sample, out of 63 systems in *HIFLUGCS*, for two we have to use estimated temperatures based on the  $L - T$  relation by Markevitch (1998). We have checked, however, that excluding these two systems from the fit does not change the derived parameters of the  $M - T$  relation.

In addition, we will use also a larger sample (enlarged *HIFLUGCS*, 88 clusters), which is not strictly flux-limited, but contains only clusters with measured temperatures.

A linear regression is performed in  $\log(T)$ - $\log(M)$  space. The method allows for errors in both variables and intrinsic scatter (Akritas & Bershady 1996). We use the bisector method to determine the best-fit parameters (Isobe et al. 1990). Errors are transformed into log space by  $\Delta \log(x) = \log(e)(x^+ - x^-)/(2x)$  where  $x^+$  and  $x^-$  denote the upper and lower boundary of the quantity’s error range, respectively. The values of the fit parameters are given in Table 1.

The results, obtained for the flux-limited and the enlarged sample agree within the uncertainty of the fit. A correction for the observed redshift does not result in any

**Table 1.** Fit parameter values for the  $M - T$  relation<sup>†</sup>.

sample	slope	norm, 1 keV $10^{13} M_{\odot}$
<i>HIFLUGCS</i>		
flux-limited	$1.676 \pm 0.054$	$3.53^{+0.33}_{-0.30}$
enlarged	$1.636 \pm 0.044$	$3.74^{+0.29}_{-0.27}$
flux-limited, $\rho_{\text{crit}} = \rho_{\text{crit}}(z)$	$1.679 \pm 0.054$	$3.52^{+0.33}_{-0.31}$
enlarged, $\rho_{\text{crit}} = \rho_{\text{crit}}(z)$	$1.636 \pm 0.046$	$3.74^{+0.29}_{-0.27}$
Sample with $kT$ -profiles		
entire sample	$1.78^{+0.09}_{-0.09}$	$2.61^{+0.38}_{-0.33}$
entire sample, $\rho_{\text{crit}} = \rho_{\text{crit}}(z)$	$1.78^{+0.10}_{-0.09}$	$2.64^{+0.39}_{-0.34}$
$M > 5 \times 10^{13} M_{\odot}$	$1.58^{+0.06}_{-0.07}$	$3.57^{+0.41}_{-0.35}$
$\beta > 0.4$	$1.58^{+0.05}_{-0.05}$	$3.57^{+0.27}_{-0.26}$
Implying isothermality to sample with $kT$ -profiles		
entire sample	$1.89^{+0.10}_{-0.09}$	$2.45^{+0.37}_{-0.32}$
$M > 5 \times 10^{13} M_{\odot}$	$1.74^{+0.07}_{-0.06}$	$3.04^{+0.29}_{-0.29}$
$\beta > 0.4$	$1.66^{+0.05}_{-0.04}$	$3.50^{+0.21}_{-0.23}$

<sup>†</sup> Errors are given at the 68% confidence level. A bootstrap method is used to estimate the errors.

change in the derived parameters. The derived slope of the  $M - T$  relation is steeper than the value of 1.5, expected from self-similar scaling relations. The normalization obtained in the hydrodynamical/ $N$ -body simulations of Evrard et al. (1996) is higher than found here. No break in the  $M - T$  relation is visible over the whole range of temperatures.

Note, however, that the determination of the mass value itself depends on the temperature, therefore some care has to be taken in the interpretation of the fit results. In the discussion, which follows below, we take this effect into account.

## 2.2. The sample with known temperature gradients.

To derive the total masses for the clusters in this sample, we use the spatially resolved temperature profiles found in ASCA measurements (Markevitch et al. 1998, Finoguenov & Ponman 1999, Finoguenov, David & Ponman 2000, hereafter FDP, FAD, Finoguenov, Jones & Böhringer 2001). The sample totals 39 systems with temperatures from 0.7 keV to 10 keV. This corresponds to a factor of 100 difference in total mass, determined at a given overdensity. A major difference of this sample, compared to studies of Horner et al. (1999) and Nevalainen et al. (2000), is an inclusion of 22 systems with temperatures spanning the range from 0.7 keV to 3.5 keV. This sample is therefore well suited to study the possible break in the  $M - T$  relation, suggested by Nevalainen et al. (2000).

In calculating the total cluster masses we used polytropic indices to describe the temperature profiles, omitting the cluster core, where effects of cooling may be important. For the total mass estimates, we used the fits to the surface brightness profiles from ROSAT PSPC data on the outskirts of the clusters from Vikhlinin et al. (1999), FDP, FAD, Finoguenov, Jones, Böhringer (2001), thus avoiding the cooling zone of the cluster. We estimate the uncertainty of surface brightness profile fitting on the mass estimation as 4% and propagate this error to the total mass. The uncertainties in the total mass estimations are much larger and are due to the uncertainty in temperature estimates and temperature gradients.

There could be a systematic effect in the analysis of ROSAT surface brightness profiles of groups, caused by variation of the ROSAT countrate-to-emission measure conversion factor at low emission temperatures (Böhringer 1996; Finoguenov et al. 1999). To evaluate this effect, we compare our fits to ROSAT surface brightness profiles with the spectral normalizations, derived in our 3d modeling of ASCA data. The latter accounts for both temperature and metallicity effects, but has larger systematics due to the complex PSF. From a good agreement, found in this comparison, a possible systematics in the total mass calculation, resulting from our approach to measuring the  $\beta$  values, is constrained to be less than 10%.

Under the assumption of hydrostatic equilibrium, when the density profile is described by a  $\beta$ -model and the temperature distribution is expressed in polytropic form ( $T(r) \propto n_{\text{gas}}^{\gamma-1}$ ), the total mass within the radius  $r = xr_c$  is simply

$$M_{\text{tot}}(< r) = 3.70 \times 10^{13} M_{\odot} T(r) r \frac{3\beta\gamma x^2}{1+x^2} \quad (1)$$

We employed Eq.1 for our mass measurements. In Table 2 we list our mass determinations at overdensity 500. Columns denote system (1), redshift (2), emission weighted temperature (3), temperature at  $r_{500}$  (4), total mass within  $r_{500}$  in  $10^{14} M_{\odot}$  (5), measured  $r_{500}$  in Mpc (6), beta and core radius (7–8). Temperature gradients are tabulated in col. (9), expressed as polytropic indices ( $\gamma$ ). In col. (10) we cite the outer radii included in the analysis of ASCA data. All errors in this table are given at the 68% confidence level.

In calculating the emission-averaged temperatures we removed the effects of cooling flows and emission lines. Thus, these temperatures are not subject to effects discussed in Mathiesen & Evrard (2000, hereafter ME00). The deviation of the measured  $M - T$  relation relative to the simulated one could be characterized by observing a *higher* temperature for a given mass. If a distinction exists between the spectral temperature measurements and the mass-averaged temperatures, as discussed in ME00, the above-mentioned discrepancy should only increase. This, however, is not true in the case of decreasing temperature profiles. We will return to this issue below.

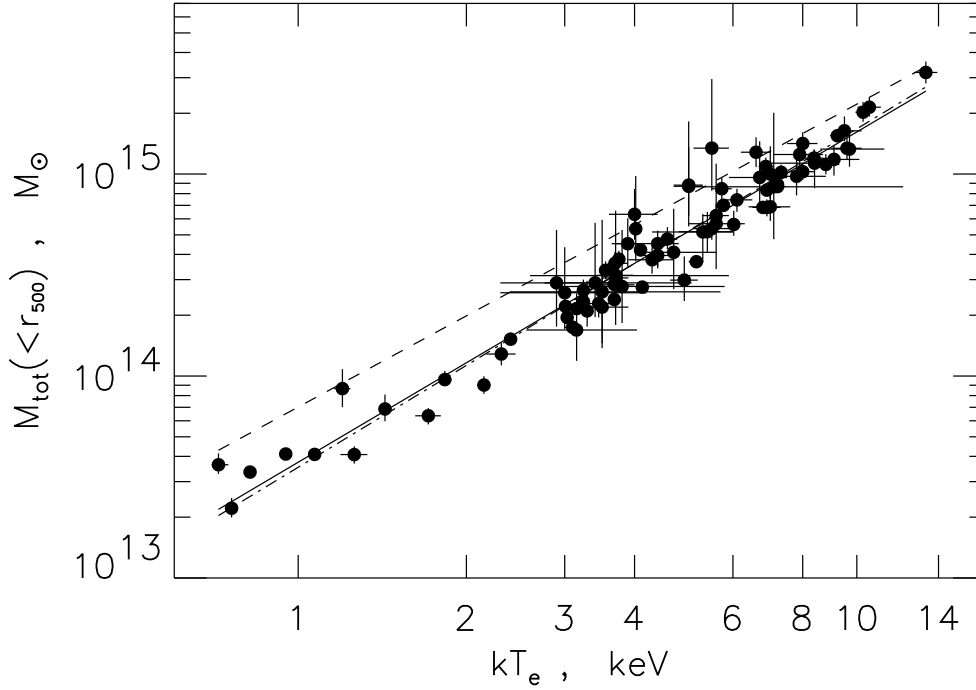


**Fig. 1.**  $M - T$  relation for the enlarged *HIFLUGCS* (filled circles indicate the data with solid line indicating the best-fit). For comparison, the fit to the  $M - T$  relation for the flux-limited *HIFLUGCS* is also shown (dot-dashed line). The dashed line shows the result of simulations by Evrard et al. (1996).

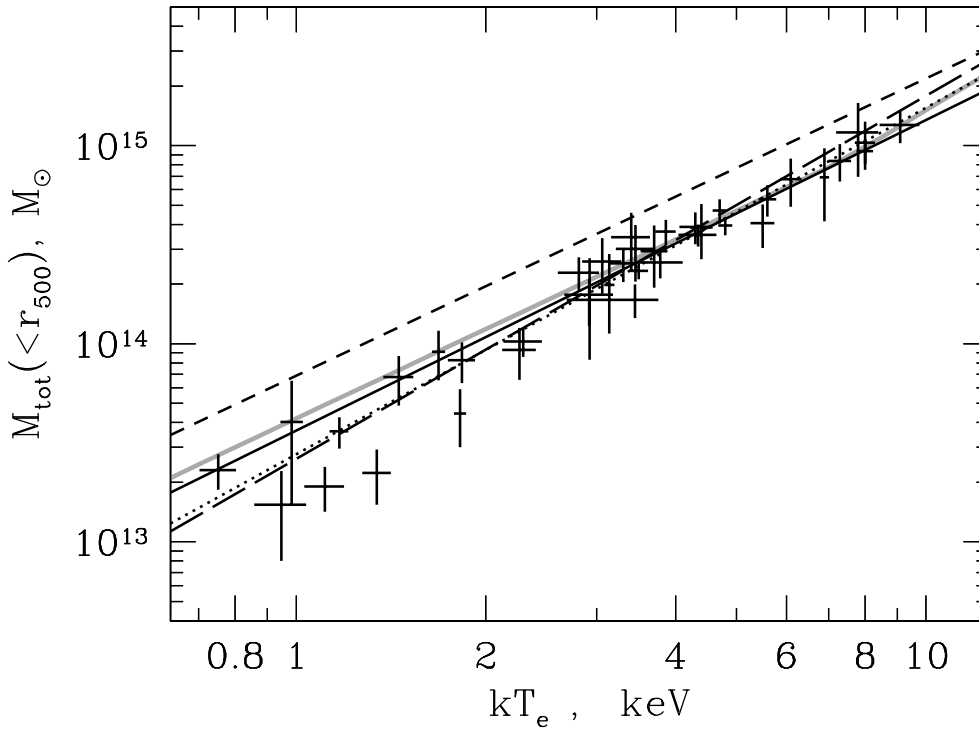


**Fig. 2.**  $M - T$  relation (analog to Fig.1) for the sample with temperature profiles. Crosses represent the mass determinations using ASCA temperature profiles and ROSAT surface brightness profile fitting. The dotted line denotes the best fit using the total sample, while the solid line denotes the best fit, when groups ( $M_{500} < 5 \times 10^{13} M_{\odot}$ ) are excluded from the fitting. The dashed line shows the result of simulations by Evrard et al. (1996). The long-dashed line shows the fit for the low-temperature end of the sample ( $kT_{ew} < 4.5$  keV). The grey line shows the effect of SN preheating on the  $M - T$  relation, discussed in FAD.

### 2.3. $M - T$ relation from spatially resolved temperatures.

In this section we investigate how the resulting parameters describing the  $M - T$  relation depend on the selection of the sample, with the most important results listed in Table 1.

Without the correction for the observed redshift the fit to the  $M - T$  relation using the bisector method by Akritas & Bershady (1996) gives

$$M_{500} = (2.61^{+0.38}_{-0.33})10^{13} \times kT_{ew}^{1.78^{+0.09}_{-0.09}}.$$

All the errors for the  $M - T$  relation reported in this section were calculated from 10000 bootstrap realizations. The mass is expressed in  $M_{\odot}$  and the temperature in keV.

0.14, 90% confidence interval is cited) at an overdensity of 1000.

Horner et al. (1999) find a flatter  $M - T$  relation, consistent with a value of 1.5, but their sample lacks groups. Nevalainen et al. (2000) suggest on the basis of their comparison of the  $M - T$  relation, derived for hot clusters and adding a few groups, that there might be a break in the  $M - T$  relation, occurring below 4 keV. Since our data uniquely sample a temperature range from groups to clusters of galaxies, we are in a position to check this suggestion.

The  $M - T$  relation derived without groups ( $M_{500} > 5 \times 10^{13} M_{\odot}$ ) is

$$M_{500} = (3.57^{+0.41}_{-0.35})10^{13} \times kT_{ew}^{1.58^{+0.06}_{-0.07}}.$$

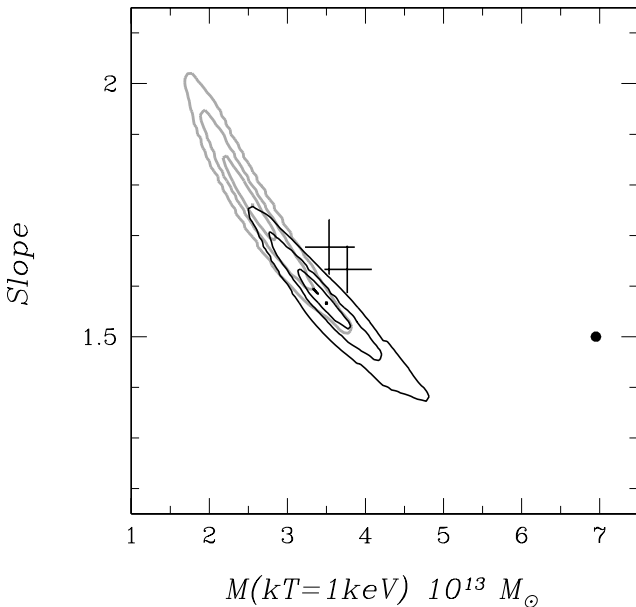


**Fig. 3.** Parameters of the bisector fit to the  $M - T$  relation. Contours, drawn at 1,2 and 3  $\sigma$  confidence level, denote the parameters derived from the sample with temperature profiles. In grey we show the fit to all the data and in black those excluding the groups ( $M_{500} < 5 \times 10^{13} M_{\odot}$ ). The black point shows the value obtained in simulations of Evrard et al. (1996), while the black crosses denote the values obtained for the enlarged and flux-limited *HIFLUGCS* sample with the error bars shown at the 68% confidence intervals.

Correcting for the redshift we obtain

$$M_{500} = (2.64^{+0.39}_{-0.34})10^{13} \times kT_{ew}^{1.78^{+0.10}_{-0.09}}.$$

Thus, there is no significant effect due to the redshift correction for our sample, composed from nearby objects, and we will omit it in further relations.

Our results on the slope of the  $M - T$  relation are in agreement with findings of Nevalainen et al. (2000), who determined a significantly steeper slope than 1.5 ( $1.79 \pm$

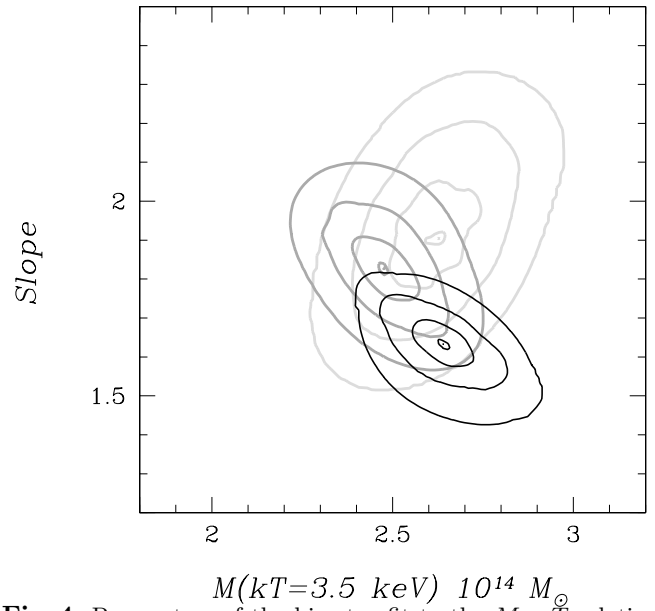


**Fig. 4.** Parameters of the bisector fit to the  $M - T$  relation, derived from the sample with temperature profiles. Light grey contours describe the slope and normalization of the  $M - T$  relation for clusters with temperature below 4 keV. In grey we show the fit to all the data and in black those excluding the groups ( $M_{500} < 5 \times 10^{13} M_{\odot}$ ). Contours are drawn at 1,2 and 3  $\sigma$  confidence level. The innermost contour marks the center.

Note that it is more straightforward to operate in terms of mass in separating the groups, since their temperatures are strongly affected by even a slight degree of preheating (Loewenstein 2000; Tozzi, Scharf & Norman 2000).

Restricting ourselves to the systems with temperatures above 3 keV, the fit is

$$M_{500} = (4.22^{+0.85}_{-0.66})10^{13} \times kT_{ew}^{1.48^{+0.10}_{-0.12}}.$$

The low-temperature end of the  $M - T$  relation (systems with temperatures below 4.5 keV) yields

$$M_{500} = (2.45^{+0.44}_{-0.39})10^{13} \times kT_{ew}^{1.87^{+0.15}_{-0.14}}.$$

The above fits and the data are shown in Fig.2. The parameters of the fits are compared with the results for the *HIFLUGCS* and simulations of Evrard et al. (1996) in Fig.3.

To study the confidence area of the parameter estimation for the above fits, we choose a normalization at 3.5 keV, which makes the determination of the slope less dependent on the normalization. We present the values derived this way in Fig.4. It can be seen from this figure that the total sample is inconsistent with a power law index of 1.5 on more than 99.9% level. The high-temperature system sample (excluding groups), although revealing a flatter index consistent with a value of 1.5, is not strongly deviant from the total sample, *e.g.* the break in the  $M - T$  relation has only 95% confidence. A steeper slope, derived for the low-temperature end of the sample, can still be considered as a fluctuation. However, larger errors in the parameter determination in the case of inclusion of groups are due to the large spread of groups on the  $M - T$  relation (see Fig.2). So, the meaning of “fluctuation” is that a subsample of systems leading to a derivation of the flat slope could be drawn from the existing sample at a high probability. The origin of the scatter is further discussed in Sec.5.

In many studies the virial radius is suggested as a unit of length (*e.g.* Evrard et al. 1996; Markevitch et al. 1998; Cen & Ostriker 1999) to provide a comparison among the systems at equal overdensity. For these estimations, the luminosity averaged temperature of the cluster is used (Markevitch et al. 1998, FDP). Therefore, we provide here a relation between  $r_{500}$  and the luminosity-weighted X-ray temperature, derived from the data in Table 2:

$$r_{500} = 0.63^{+0.01}_{-0.01} \times \sqrt{kT_{ew}},$$

where  $r_{500}$  is in Mpc and  $kT_{ew}$  in keV. For a given temperature this relation implies a 20% smaller value for  $r_{500}$  compared to similar formulae derived from the simulations of Evrard et al. (1996).

### 3. Polytropic vs Isothermal

As given in Eq.1, the deduced mass depends on the temperature and the parameters  $\beta$  and  $\gamma$ , describing the shape of the density and temperature profile. To further elucidate the origin of the behavior of the  $M - T$  relation and to circumvent the direct dependence of  $M$  on  $T$  we examine in Fig.5 the dependence of  $\beta$  (correctly  $\beta x^2/(1+x^2)$  at  $r_{500}$ ) on  $T$ . We note four systems with  $\beta \sim 0.3$  that imply a steep dependence of beta on the temperature. They are mainly responsible for the steep slope of the  $M - T$  relation in our sample with spatially resolved temperatures. In fact, excluding these systems (IC4296, HCG62, HCG51, NGC3258), but leaving other groups in, the  $M - T$  relation is given by

$$M_{500} = (3.57^{+0.27}_{-0.26})10^{13} \times kT_{ew}^{1.58^{+0.05}_{-0.05}}.$$

Excluding two more systems (A262, HCG94), whose  $\beta$ -index is less than 0.5, no further changes in the derived parameters of the  $M - T$  relation are obtained:

$$M_{500} = (3.75^{+0.29}_{-0.25})10^{13} \times kT_{ew}^{1.56^{+0.05}_{-0.05}}.$$

All of the three groups in a sample of Nevalainen et al. (2000) have a  $\beta$ -index less or equal to 0.5. The above demonstrates the importance of selection effects on the derived slope of the  $M - T$  relation, especially on the group scale, originating from apparent scatter in the  $M - T$  relation on the scales of groups. Observationally, this scatter is correlated with flat gas density profiles, which are often taken for signs of preheating (Metzler & Evrard 1997). In reality, the situation is more complex, since as pointed out by Loewenstein (2000), when the effect of the SN feedback is the only one responsible for the observed  $M - T$  relation, in low-mass systems, a large amount of metals associated with SN explosions should be observed and also isentropic cores, corresponding to the case of adiabatic collapse. Although some of the groups do show such features (Finoguenov et al. 2001), these are surprisingly not the most deviant systems in the  $M - T$  relation.

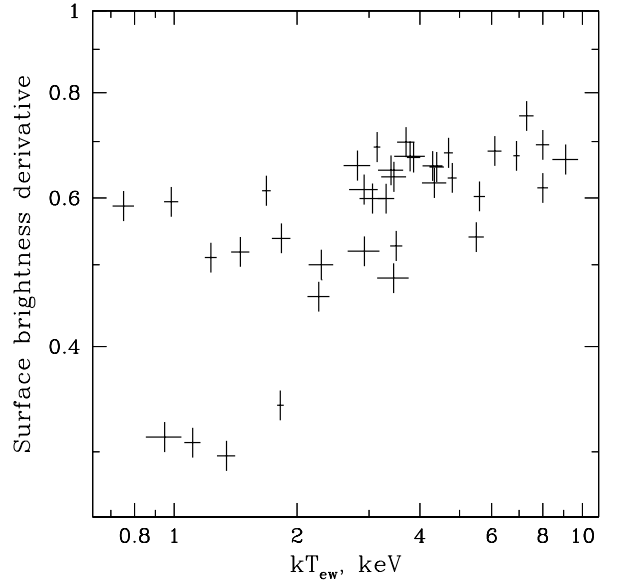


**Fig. 5.** Relation between density gradient (defined by  $\beta x^2/(1+x^2)$ ) and  $T_{ew}$ .

Horner et al. (1999) have found that the dependence of  $\beta$  on  $T_{ew}$  is responsible for the steepening of the derived  $M - T$  in the isothermal assumption, but when the temperature profiles are taken into account, the slope becomes 3/2 again. To verify this, we rewrite Eq.1 in terms of overdensity

$$M(\delta, \beta, \gamma, T(\delta)) \approx 2.2 \times 10^{15} M_{\odot} \delta^{-1/2} \beta^{3/2} \gamma^{3/2} T(\delta)^{3/2}, \quad (2)$$

where  $\delta$  denotes the chosen overdensity. If the idea of Horner et al. (1999) is correct, Eq.2 should contain a term counterbalancing the dependence of  $\beta$  on  $T_{ew}$ , with possibilities  $\gamma \propto T_{ew}^{\alpha}$ ,  $T(\delta)/T_{ew} \propto T_{ew}^{\alpha}$  or both. The index

$\alpha$  of this (counter-)dependence is  $-0.26 \pm 0.03$  according to Horner et al. (1999), but weaker dependences of  $\beta$  on  $T$  are also reported (e.g. 0.16 in Vikhlinin et al. 1999).

As is seen from Figs.6 and 7, the data show two trends, which cancel each other: both very hot and very cold systems seem to have stronger temperature gradients. So, the trend on the high-energy part counterbalances the weak dependence of  $\beta$  on  $T$ , while the trend in the low-temperature part only reinforces the trend observed in  $\beta$ . Thus, it becomes clear why inclusion of groups makes such a drastic difference in the derived  $M - T$  relation. An overall fit to these figures gives  $\gamma = (1.080 \pm 0.005) T_{ew}^{(-0.010 \pm 0.004)}$  and  $T(\delta)/T_{ew} = (0.88 \pm 0.18) T_{ew}^{(-0.03 \pm 0.14)}$ .

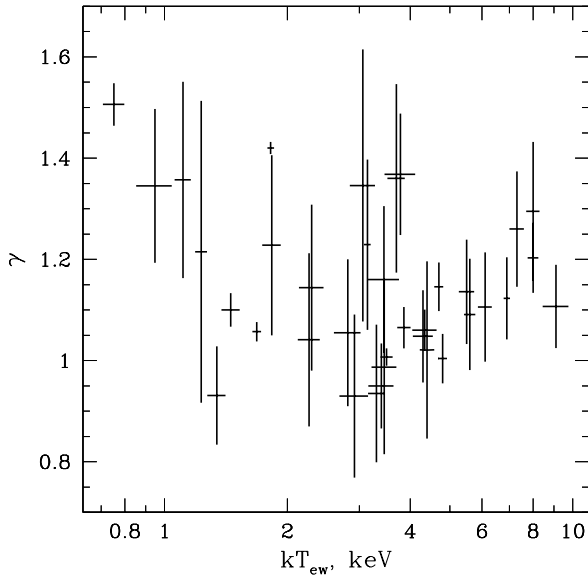


**Fig. 6.** Relation between  $\gamma$  and  $T_{ew}$ . The data are shown as crosses with error bars drawn at the 68% confidence level.

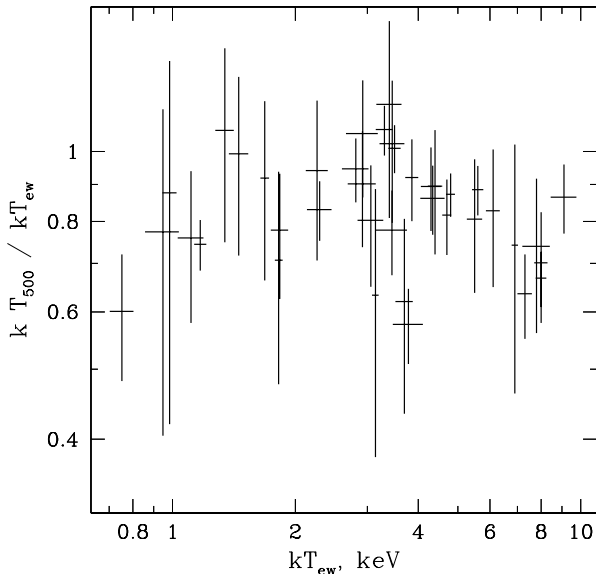


**Fig. 7.** Relation between  $T_{500}/T_{ew}$  and  $T_{ew}$ .

In fact, the arguments presented in Horner et al. (1999) are not strictly correct. They base their conclusion on the fact that

$M(\beta)/M(True) \propto r^{0.4}$  for an individual cluster, where  $M(\beta)$  is the mass estimate using the  $\beta$ -model and assuming isothermality and  $M(True)$  is the true mass of the cluster.

However, what is relevant is:

$M(\beta)/M(True) \propto (r/r_{core})^{0.4}$  for the cluster sample,  $r_{core} \propto r(\delta) \propto T^{0.5}$  where  $r_{core}$  is the cluster core radius and  $r(\delta)$  is the radius of overdensity  $\delta$ ,

from which it follows:

$M(\beta)/M(True) \propto (r(\delta)/r_{core})^{0.4} \propto (T^{0.5}/T^{0.5})^{0.4} = constant$ .

This means that if clusters are self similar, the overestimate of the beta model is the same for all clusters. In view of this consideration, we note that there is a very close agreement between the parameters of the  $M - T$  relation determined in our two samples. This agreement, which demonstrates that usage of the isothermality assumption does not bias the derived parameters of the  $M - T$  relation, derived for high-redshift samples, where detailed temperature measurements are difficult and an assumption of isothermality is the only choice.

Following a suggestion of the referee, we examine also the effect of assuming isothermality in deriving the total mass for the sample with spatially resolved temperature measurements. The results are listed in Table 1. The slope of the  $M - T$  relation, obtained for the total sample, is still steeper, while avoiding the systems with flat  $\beta$  gives results consistent with *HIFLUGCS* in both slope and normalization. We note that the lowest  $\beta$  value for the *HIFLUGCS* sample is 0.44, which again supports the idea of the importance of the selection of the systems with respect to their values of  $\beta$ .

Concluding this section, we identify the inclusion of systems with low values of  $\beta$  as the most important cause of the steep slope of the  $M - T$  relation, which could be overcome by excluding such systems from the sample. As we have shown, a flat  $\beta$  is not necessarily a unique characteristic of groups, which most likely implies a different importance of preheating in low-mass systems. This is in qualitative agreement with the preferential infall scenario, proposed by FAD.

In all the fits, however, the normalization of the  $M - T$  relation appears smaller than in the simulations of Evrard et al. (1996). In the following, we would like to comment on this issue. As pointed out by Nevalainen et al. (2000), the resolution in the simulations of Evrard et al. (1996) is insufficient to resolve the cluster cores. One can assume, however, that their simulations are correct at low overdensities. Since we measure the temperature up to the radius of the overdensity chosen for the mass calculations, we can directly check this effect by using a temperature at the radius of mass determination, ( $T_{500}$ ),

instead of the luminosity-weighted temperatures. Such a comparison may also be less affected by preheating, since at  $\delta = 500$  no significant variation in the gas fraction is seen (Ettori & Fabian 1999, Vikhlinin et al. 1999). Taking measured temperatures also avoids many possible effects of averaging, discussed in ME00 and is therefore closer to the relations predicted for the mass-weighted temperature. A fit to the  $M_{500} - T_{500}$  relation reads as

$$M_{500} = (3.29^{+0.61}_{-0.59})10^{13} \times kT_{500}^{1.89^{+0.16}_{-0.14}},$$

(errors are stated at the 68% confidence level).

The normalization of  $M - T_{500}$  in the simulations by Evrard et al. (1996) is about  $9. - 15. \times 10^{13} M_{\odot}$  (considering  $T_{500} = 0.6 - 0.8 T_X$ ), closer to the observed points, but still in obvious disagreement (fixing the slope to 1.5 we obtain a normalization at 1 keV of  $4.81^{+0.30}_{-0.29} \times 10^{13} M_{\odot}$ ).

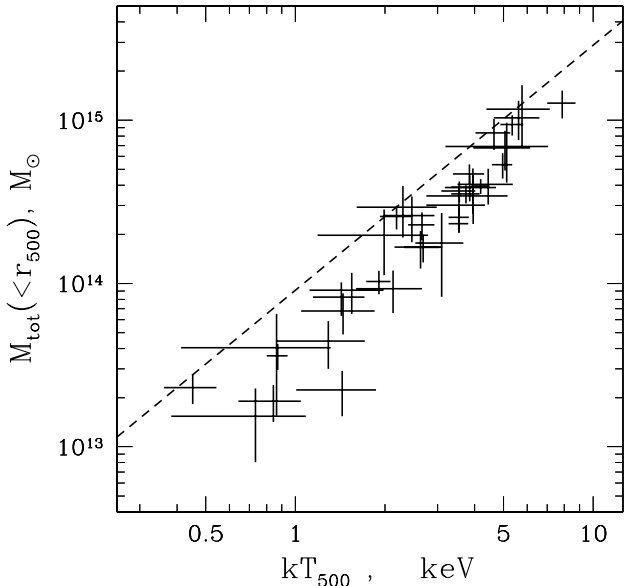


**Fig. 8.**  $M_{500} - T_{500}$  relation. Dashed line shows the rescaled simulations by Evrard et al. (1996).

#### 4. Comparison with optical data

Comparison between the X-ray and the virial mass measurements, obtained using velocity dispersions, is long known to be subject to contradictions, with velocity bias considered as the most likely origin. Recently, a new compilation of optical measurements was made by Girardi et al. (1998), where a much more detailed study was carried out, *e.g.* different velocity dispersion profiles in clusters were identified. Since we have measured the masses for many clusters in common, we can combine the X-ray mass with velocity dispersion measurements to provide a comparison with high-resolution dark matter simulations.

We take high-resolution  $\Lambda$ CDM ( $\Omega_M = 1 - \Omega_{\Lambda} = 0.3$ ,  $\sigma_8 = 1.0$ ;  $H_0 = 70 \text{ km s}^{-1} \text{ Mpc}^{-1}$ ) simulations using the ART code (Kravtsov, Klypin, Khokhlov 1997), with  $256^3$  particles of  $1.1 \times 10^9 M_{\odot}$  each in a simulation box of

$60h^{-1} \text{ Mpc}$  (see Gottloeber et al. 1999 for details). The particular runs of the ART code we use for comparison are characterized by a scale of velocity dispersion with overdensity of  $\sigma_P \propto \delta^{0.06}$  with a residual scatter around the best-fit of 20–30%. Within the simulated box, 17 clusters have been identified and we build the  $M - \sigma_P$  relation, scaling the measurements done at different overdensities. One possible weakness of such a comparison is that in the simulations we have studied the dispersion of the dark matter, not of the galaxies.

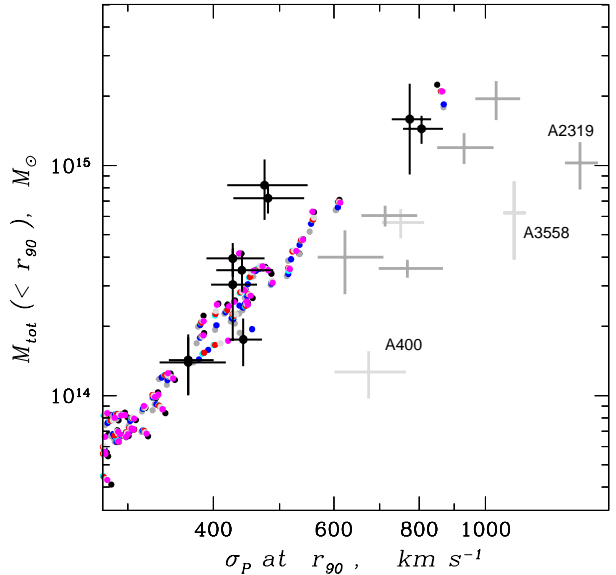


**Fig. 9.**  $M - \sigma_P$  relation at overdensity of 90. Circles represent the results of high-resolution simulations. Black crosses represent a correlation of the X-ray mass measurements with the velocity dispersion of galaxies at overdensity of 90. Type A clusters (Girardi et al. 1998) are shown in black, type B in grey and C in light grey (this identification has been made to denote different velocity dispersion profiles measured in these clusters, which reflect, according to Girardi et al. (1998), that type B and C cluster have been formed earlier and are therefore more relaxed).

Optical observations reveal 3 types of clusters, according to their degree of virialization. In comparing the data, we have scaled the optical velocity dispersions according to the given type of cluster, using identification and scaling profiles, reported in Girardi et al. (1998). To compare our X-ray results with the work of Girardi et al. (1998), we rescale our mass estimates to the overdensity of 90, using the Navarro, Frenk & White (1996) profile.

The resulting  $M - \sigma_P$  relation is presented in Fig.9. The outliers on the  $M - \sigma_P$  relation, A2319, A3558 and A400, are already known to have a peculiar structure (Ferretti, Giovannini, Böhringer 1997; Venturi et al. 2000; Lloyd-Davies, Ponman, Cannon 2000). The scatter of the other points around the simulations is within 30% and therefore comparable to the scatter seen in simulations. We note, however, that there is a trend of type B and C clusters to have a higher velocity dispersion for a given



mass, which is consistent with a definition of their type: type B and C are older systems, according to modeling of Girardi et al. (1998), that should imply a higher formation redshift. Since such a correction is not introduced into the virial mass calculation, this results in a slight bias in mass estimates for these clusters, as seen in Fig.10.

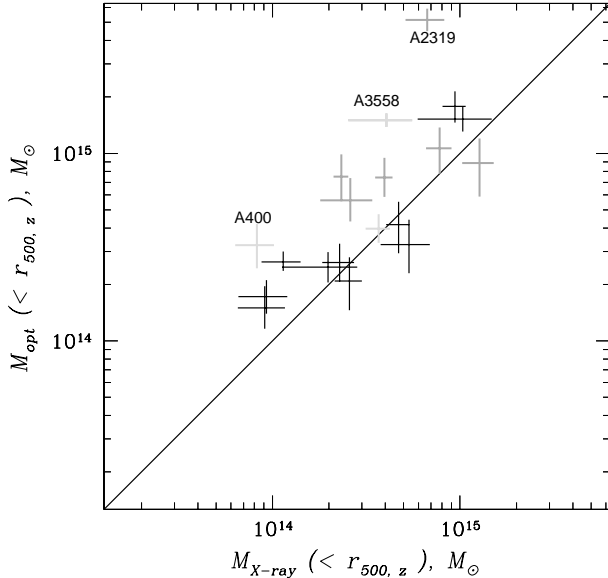


**Fig. 10.** Comparison of the X-ray and optical mass estimates. Black crosses denote type A clusters in Girardi et al. (1998), grey crosses type B and light grey crosses type C. Type A clusters show the best agreement with the X-ray mass measurements.

## 5. Implications on the Redshift (Epoch) of cluster formation

The issue of the redshift of cluster formation was strongly suggested in studies of Lilje (1992), Kitayama & Suto (1996), Voit & Donahue (1998). The effect on the  $M - T$  relation is such that for a given mass, the systems that formed at earlier times should have higher temperatures. Since this scenario is in qualitative agreement with trends observed by comparing our sample with the simulations of Evrard et al. (1996), we decided to estimate whether the shift observed in the  $M - T$  relation could be explained just by this scenario.

To do this, we invert the problem, *i.e.* use the X-ray mass and temperature measurements and the  $M - T$  relation obtained in the simulations to derive the distribution of redshifts of cluster formation for our sample. In more detail, for a measured mass of the system, we compare the measured temperature with the value obtained from the simulation for the measured mass and attribute the difference to the redshift of cluster formation, which for  $\Omega_M = 1$  is simply  $T_{observed} = T_{simulated} \times (1 + z_f)$ . To be able to do this, one should make sure that the simulated relation explicitly assumes that the clusters form at the redshift of observation. Fortunately, the simulations of

Evrard et al. (1996) have this assumption, which is quite logical for  $\Omega_M = 1$ , used for most of their runs (Metzler, private communication).

In Fig.11 we illustrate the effect of the redshift of cluster formation, by comparison with the model of Lacey & Cole (1993) following the formulae presented in Balogh et al. (1999) for  $\Omega_M = 0.3$ . We subdivide our sample into 3 parts with masses in the  $0.1 - 0.8$ ,  $0.8 - 3$  and  $3 - 15 \times 10^{14} M_{\odot}$  range. From the Figure one can see that the theoretical prediction varies significantly between the three subsets and generally matches the trends seen in the corresponding subset. While a more detailed comparison should await an  $M - T$  relation simulated with much better resolution, we can state already that a steeper slope of the observed  $M - T$  relation implies that lower-mass systems form preferentially at earlier times, compared to rich clusters. The formation redshift distribution for groups is wider than the model prediction, which can be taken as a sign of the importance of SN preheating, but a more detailed study is needed to verify this suggestion.

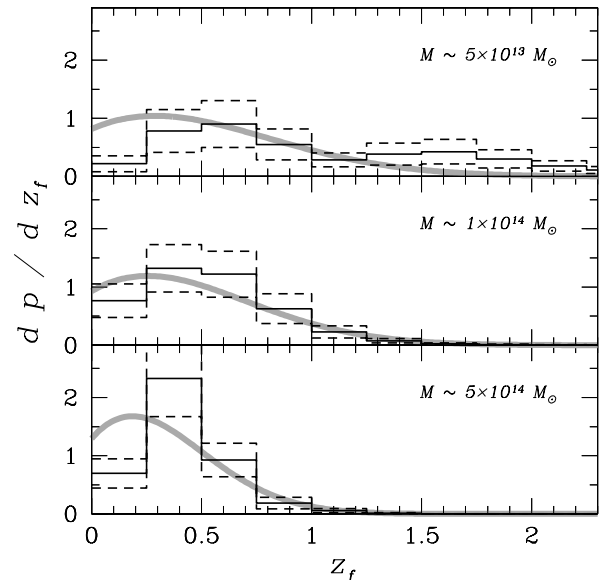


**Fig. 11.** Redshifts of cluster formation, deduced from a requirement for measurements to match the simulations of Evrard et al. (1996). The black solid histogram shows the calculation for the sample with temperature profiles with dashed histograms indicating the number count errors at the 68% confidence level. We present the comparison with the model of Lacey & Cole (1993) following the formulae presented in Balogh et al. (1999) for  $\Omega_M = 0.3$  and three mass ranges in our sample with typical masses of  $5 \times 10^{13} M_{\odot}$ ,  $1 \times 10^{14} M_{\odot}$  and  $5 \times 10^{14} M_{\odot}$  (grey lines).

We can already identify one source of bias in the formation redshift distribution of the clusters in the present study. Systems that collapsed recently bear indications of recent merger activity and therefore are selectively removed from the sample aimed to determine the mass using the assumption of hydrostatic equilibrium. Therefore, the first bin in the derived  $z_f$  distribution should be

disregarded in Fig.11. Flux-limited samples, such as *HIFLUGCS*, are in principle also biased in this regard, since older systems are expected to be brighter for a given mass. The lack of clusters lying close to the simulations on the  $M - T$  plane is also caused by influence of a central region on the determination of the luminosity averaged temperature, since formation of the central part of a cluster is slightly shifted towards higher formation epochs.

## 6. Conclusions

We have studied the  $M - T$  relation using a sample of clusters with resolved temperature profiles and also using *HIFLUGCS*. Our findings are

- Using spatially resolved temperatures in mass estimates results in similar parameters of the  $M - T$  relation to the analysis assuming isothermality. The observed slope of the  $M - T$  relation is steeper than the predictions of the self-similar relations and the measured normalization is two times lower than that obtained in the simulations of Evrard et al. (1996).
- Significant scatter of the points on the  $M - T$  relation was found for groups. This is a likely source of the disagreement found between the studies of Nevalainen et al. (2000) and Horner et al. (1999).
- We find that the derived slope of the  $M - T$  relation depends strongly on the  $\beta$  dependence on temperature and is not counterbalanced by inclusion of temperature gradients, as proposed by Horner et al. (1999). This provides an explanation for similar parameters of the  $M - T$  relation, derived using temperature profiles, compared to the method employing the assumption of isothermality, as in the *HIFLUGCS* sample.
- We conclude that the deviation of the measured  $M - T$  relation from the simulated one is due to the combined effect of preheating and the difference between observed redshift and epoch of cluster formation. Avoiding clusters with signs of recent merger activity in a sample selected for mass estimates biases the sample toward earlier formation epochs.
- To avoid the effects of preheating, we combine X-ray mass measurements with galaxy velocity dispersion measurements of Girardi et al. (1998) to build an  $M - \sigma_P$  relation, which we compare with high-resolution dark matter simulations. Apart from obvious outliers, also identified in other studies, there is a clear difference between different cluster types, derived according to velocity dispersion profile. In type B and C clusters, identified as most relaxed, the velocity dispersion is highest for a given mass, in qualitative agreement with predictions from models accounting for the epoch of cluster formation.

## Acknowledgments

The authors thank Stephan Gottloeber for providing the results of simulations using ART code. AF acknowledges useful conversations with Monique Arnaud, Stefano Ettori, Yasushi Ikebe, Maxim Markevitch, Chris Metzler, Volker Mueller and Alexey Vikhlinin during preparation of this paper. AF acknowledges support from Alexander von Humboldt Stiftung and NASA grant NAG5-3064 during preparation of this work. The authors thank the anonymous referee for useful comments on the manuscript. The authors acknowledge the devoted work of the ROSAT and ASCA operation and calibration teams, without which this paper would not be possible.

## References

- Akritas M.G. and Bershadsky M.A., 1996, ApJ, 470, 706  
 Allen S.W., 1998, MNRAS, 296, 392  
 Balogh M.L., Babul A., Patton D.R., 1999, MNRAS, 307, 463  
 Böhringer H., 1995, in Large Scale Structure in the Universe, J.P. Mücke, S. Gottlöber, V. Müller (eds.), World Scientific, Singapore, 181  
 Böhringer H., 1996, in Röntgenstrahlung from the Universe, H.U. Zimmermann, J.E. Trümper, H. Yorke (eds.), MPE Report No. 263, 537  
 Borgani S., Girardi M., Carlberg R. G., Yee H. K. C., Ellingson E., 1999, ApJ, 527, 561  
 Cavaliere A. and Fusco-Femiano R., 1976, A&A, 49, 137  
 Cen R., Ostriker J. P., 1999, ApJ, 519, L109  
 Colín C., Klypin, A., Kravtsov A., Khokhlov A., 1999, ApJ, 523, 32  
 Collins C.A., Guzzo L., Böhringer H., Schuecker P., Chincarini G. et al. , 2000, MNRAS accepted, (astro-ph/0008245)  
 Eke V., Cole S. and Frenk C., 1996, 282, 263  
 Eke V., Cole S., Frenk C., Henry P.J., 1998, MNRAS, 298, 1145  
 Ettori S., Fabian A., 1999, MNRAS, 305, 834  
 Evrard A.E., Metzler C.A., Navarro J.F., 1996, ApJ, 469, 494  
 Evrard A.E., 1997, MNRAS, 292, 289  
 Feretti L., Giovannini G., Böhringer H., 1997, New Astronomy, 2, 501  
 Finoguenov A., Jones C., Forman W. and David L., 1999, ApJ, 514, 844  
 Finoguenov A. and Ponman T.J., 1999, MNRAS, 305, 325  
 Finoguenov A., David L.P., Ponman T.J., 2000, ApJ, 544, 188; FDP  
 Finoguenov A., Arnaud M., David L.P., 2000, ApJ accepted, (astro-ph/0009007); FAD  
 Finoguenov A., Jones C., Böhringer H., 2001, ApJ in preparation  
 Fukazawa Y., Nakazawa K., Isobe N., Makishima K., Matsushita K., Ohashi T., Kamae T., 2000, ApJ, accepted, (astro-ph/0011257)

- Girardi M., Giuricin G., Mardirossian F., Mezzetti M., Boschin W., 1998, *ApJ*, 505, 74
- Gottloeber S., Klypin A., Kravtsov A., Turchaninov V., 1999, preprint astro-ph/9909185
- Gorenstein P., Fabricant D., Topka K., Harnden Jr. F.R., Tucker W. H., 1978, *ApJ*, 224, 718
- Henry J.P., Arnaud K.A., 1991, *ApJ*, 372, 410
- Henry J.P., Gioia I.M., Maccacaro T., Morris S.L., Stocke J.T., Wolter A., 1992, *ApJ*, 386, 408
- Hjorth J., Oukbir J., van Kampen E., 1998, *MNRAS*, 298, 1
- Horner D.J., Mushotzky R.F., Scharf C.A., 1999, *ApJ*, 520, 78
- Irwin J.A., Bregman J.N., Evrard A.E., 1999, *ApJ*, 519, 518
- Isobe T., Feigelson E.D., Akritas M.G., Babu G.J., 1990, *ApJ*, 364, 104
- Jones C., Forman W.R., 1984, *ApJ*, 276, 38
- Kitayama T., Suto Y., 1996, *ApJ*, 469, 480
- Kravtsov A., Klypin A., Khokhlov A., 1997, *ApJS*, 111, 73
- Lacey C., Cole S., 1993, *MNRAS*, 262, 627
- Lilje P.B., 1992, *ApJ*, 386, L33
- Lloyd-Davies E.J., Ponman T.J., Cannon D.B., 2000, *MNRAS*, 315, 689
- Loewenstein M., 2000, *ApJ*, 532, 17
- Markevitch M., Forman W. R., Sarazin C. L., & Vikhlinin A. 1998, *ApJ*, 503, 77
- Markevitch M., 1998, *ApJ*, 504, 27
- Mathiesen B.F., Evrard A.E., 2000, preprint astro-ph/0004309; ME00
- Metzler C.A., Evrard A.E., 1997, preprint astro-ph/9710324
- Miller C.J., Batuski D.,J., 2000, *ApJ* submitted, (astro-ph/0002295)
- Mushotzky R.F., Serlemitsos P.J., Smith B.W., Boldt E.A., & Holt S.S., 1978, *ApJ*, 225, 21
- Mushotzky R.F. 1984, *Phys. Scr.* T7, 157
- Navarro J.F., Frenk C.S. & White S.D.M., 1996, *ApJ*, 462, 563
- Nevalainen J., Markevitch M., & Forman W., 2000, *ApJ*, 536, 73
- Nichol R.C., Collins C.A., Guzzo L., Lumsden S.L., 1992, *MNRAS*, 255, 21
- Oukbir J., Blanchard A., 1992, *A&A*, 262, 21
- Press W.H., Schechter P., 1974, *ApJ*, 187, 425
- Reiprich et al. , 2001, *A&A* in preparation
- Retzlaff J., Borgani S., Gottlobber S., Klypin A., Müller V., 1998, *NewA*, 3, 631
- Romer A.K., Collins C.A., Böhringer H., Cruddace R.C., Ebeling H., MacGillivray H.T., Voges W., 1994, *Nature*, 372, 75
- Schindler S., *A&A*, 1996, 305, 756
- Schuecker P., Böhringer H., Guzzo L., Collins C.A., Neumann D.M. et al. , 2000, *A&A* accepted, astro-ph/0012105
- Tozzi P., Scharf C., Norman C., 2000, *ApJ*, 542, 106
- Vikhlinin A., Forman W., Jones C., 1999, *ApJ*, 525, 47
- Venturi T., Bardelli S., Morganti R., Hunstead R.W., 2000, *MNRAS*, 314, 594
- Voit G.M., Donahue M., 1998, *ApJ*, 500, L111
- White D.A., 2000, *MNRAS*, 312, 663

**Table 2.** Mass determinations using spatially resolved temperatures.

Name	$z$	$kT$ keV	$kT_{500}$ keV	$M_{500}$ $10^{14} M_{\odot}$	$r_{500}$ Mpc	$\beta$	$r_{core}$ Mpc	$\gamma$	$R_{out}$ Mpc
A2029	0.077	$9.10 \pm 0.66$	$7.87 \pm 0.86$	$12.71 \pm 2.44$	$2.06 \pm 0.27$	0.68	0.28	$1.11 \pm 0.08$	2.82
A401	0.074	$8.00 \pm 0.24$	$5.34 \pm 0.47$	$9.40 \pm 1.32$	$1.70 \pm 0.16$	0.63	0.27	$1.20 \pm 0.07$	1.82
A3266	0.055	$8.00 \pm 0.30$	$5.61 \pm 0.98$	$10.36 \pm 2.81$	$1.93 \pm 0.36$	0.74	0.50	$1.29 \pm 0.14$	1.57
A1795	0.062	$7.80 \pm 0.60$	$5.77 \pm 1.39$	$11.66 \pm 4.72$	$2.00 \pm 0.56$	0.83	0.39	$1.19 \pm 0.19$	1.56
A2256	0.058	$7.30 \pm 0.30$	$4.64 \pm 0.62$	$8.38 \pm 1.80$	$1.79 \pm 0.27$	0.82	0.52	$1.26 \pm 0.11$	1.83
A3571	0.040	$6.90 \pm 0.12$	$5.12 \pm 1.93$	$6.91 \pm 2.75$	$1.68 \pm 0.46$	0.69	0.27	$1.12 \pm 0.08$	2.28
A1651	0.085	$6.10 \pm 0.24$	$5.05 \pm 1.09$	$6.77 \pm 1.85$	$1.67 \pm 0.32$	0.70	0.26	$1.11 \pm 0.11$	1.62
A119	0.044	$5.60 \pm 0.18$	$4.96 \pm 0.39$	$5.34 \pm 0.95$	$1.54 \pm 0.19$	0.66	0.48	$1.09 \pm 0.11$	1.28
A3558	0.048	$5.50 \pm 0.24$	$4.44 \pm 0.93$	$4.05 \pm 1.01$	$1.41 \pm 0.24$	0.55	0.19	$1.14 \pm 0.10$	1.39
A2199	0.030	$4.80 \pm 0.12$	$4.19 \pm 0.29$	$3.95 \pm 0.41$	$1.40 \pm 0.10$	0.64	0.14	$1.00 \pm 0.05$	1.25
A496	0.033	$4.70 \pm 0.12$	$3.84 \pm 0.46$	$4.70 \pm 0.67$	$1.48 \pm 0.15$	0.70	0.25	$1.15 \pm 0.05$	1.32
A4059	0.048	$4.40 \pm 0.18$	$3.94 \pm 0.77$	$3.87 \pm 1.20$	$1.39 \pm 0.30$	0.67	0.22	$1.02 \pm 0.17$	0.92
A3112	0.075	$4.34 \pm 0.30$	$3.74 \pm 0.41$	$3.54 \pm 0.45$	$1.35 \pm 0.12$	0.63	0.12	$1.06 \pm 0.04$	1.74
Hydra	0.057	$4.30 \pm 0.24$	$3.85 \pm 0.51$	$3.89 \pm 0.71$	$1.39 \pm 0.18$	0.66	0.12	$1.05 \pm 0.09$	1.35
A2063	0.035	$3.86 \pm 0.14$	$3.55 \pm 0.46$	$3.68 \pm 0.54$	$1.36 \pm 0.14$	0.69	0.22	$1.07 \pm 0.04$	0.93
MKW3S	0.045	$3.79 \pm 0.32$	$2.18 \pm 0.26$	$2.57 \pm 0.43$	$1.21 \pm 0.14$	0.71	0.30	$1.37 \pm 0.12$	1.16
A2657	0.040	$3.70 \pm 0.18$	$2.30 \pm 0.69$	$2.93 \pm 1.02$	$1.27 \pm 0.31$	0.76	0.37	$1.36 \pm 0.19$	1.17
AWM7	0.017	$3.50 \pm 0.12$	$3.54 \pm 0.27$	$2.33 \pm 0.21$	$1.17 \pm 0.07$	0.53	0.10	$1.01 \pm 0.02$	0.75
A2052	0.035	$3.46 \pm 0.24$	$3.54 \pm 0.79$	$3.02 \pm 0.96$	$1.28 \pm 0.28$	0.64	0.10	$0.99 \pm 0.17$	0.46
HCG94	0.042	$3.45 \pm 0.31$	$2.68 \pm 0.36$	$1.67 \pm 0.32$	$1.05 \pm 0.14$	0.48	0.08	$1.16 \pm 0.14$	1.08
2A0335	0.035	$3.40 \pm 0.24$	$3.95 \pm 1.20$	$3.44 \pm 1.13$	$1.34 \pm 0.30$	0.65	0.08	$0.95 \pm 0.08$	0.92
A4038	0.028	$3.31 \pm 0.16$	$3.55 \pm 0.28$	$2.55 \pm 0.50$	$1.21 \pm 0.16$	0.61	0.16	$0.94 \pm 0.14$	0.38
A1060	0.011	$3.14 \pm 0.06$	$1.99 \pm 0.80$	$1.98 \pm 0.86$	$1.11 \pm 0.33$	0.70	0.16	$1.23 \pm 0.17$	0.31
A2634	0.031	$3.06 \pm 0.22$	$2.46 \pm 0.47$	$2.60 \pm 0.81$	$1.22 \pm 0.26$	0.69	0.45	$1.35 \pm 0.27$	0.83
MKW9	0.040	$2.92 \pm 0.26$	$3.10 \pm 0.57$	$1.77 \pm 0.94$	$1.07 \pm 0.39$	0.52	0.05	$0.97 \pm 0.45$	0.71
AWM4	0.032	$2.92 \pm 0.23$	$2.63 \pm 0.48$	$1.67 \pm 0.43$	$1.05 \pm 0.19$	0.62	0.11	$0.93 \pm 0.16$	0.46
A539	0.029	$2.81 \pm 0.21$	$2.66 \pm 0.27$	$2.28 \pm 0.44$	$1.16 \pm 0.16$	0.69	0.25	$1.05 \pm 0.14$	0.72
MKW4S	0.028	$2.29 \pm 0.16$	$1.91 \pm 0.18$	$1.03 \pm 0.17$	$0.89 \pm 0.10$	0.51	0.12	$1.14 \pm 0.16$	0.75
A262	0.016	$2.26 \pm 0.14$	$2.13 \pm 0.53$	$0.93 \pm 0.27$	$0.86 \pm 0.17$	0.46	0.06	$1.04 \pm 0.17$	0.44
A400	0.024	$1.83 \pm 0.09$	$1.43 \pm 0.28$	$0.82 \pm 0.19$	$0.83 \pm 0.13$	0.56	0.18	$1.23 \pm 0.18$	0.64
N3258	0.009	$1.82 \pm 0.04$	$1.29 \pm 0.42$	$0.45 \pm 0.14$	$0.67 \pm 0.15$	0.34	0.05	$1.42 \pm 0.01$	0.57
MKW4	0.020	$1.68 \pm 0.04$	$1.55 \pm 0.43$	$0.91 \pm 0.26$	$0.86 \pm 0.17$	0.64	0.18	$1.06 \pm 0.02$	0.66
N6329	0.028	$1.45 \pm 0.08$	$1.44 \pm 0.40$	$0.68 \pm 0.19$	$0.78 \pm 0.15$	0.53	0.12	$1.10 \pm 0.03$	0.64
HCG51	0.026	$1.34 \pm 0.07$	$1.44 \pm 0.43$	$0.22 \pm 0.07$	$0.54 \pm 0.11$	0.30	0.08	$0.93 \pm 0.10$	0.69
N5044	0.009	$1.23 \pm 0.04$	$0.87 \pm 0.07$	$0.36 \pm 0.07$	$0.63 \pm 0.08$	0.51	0.01	$1.22 \pm 0.30$	0.28
HCG62	0.014	$1.11 \pm 0.05$	$0.84 \pm 0.20$	$0.19 \pm 0.05$	$0.51 \pm 0.09$	0.31	0.02	$1.36 \pm 0.19$	0.58
N4325	0.026	$0.98 \pm 0.04$	$0.86 \pm 0.45$	$0.40 \pm 0.25$	$0.65 \pm 0.28$	0.59	0.01	$1.14 \pm 0.56$	0.60
IC4296	0.013	$0.95 \pm 0.09$	$0.73 \pm 0.35$	$0.15 \pm 0.07$	$0.47 \pm 0.16$	0.31	0.06	$1.35 \pm 0.15$	0.32
N5129	0.023	$0.75 \pm 0.05$	$0.45 \pm 0.09$	$0.23 \pm 0.05$	$0.54 \pm 0.08$	0.60	0.10	$1.51 \pm 0.04$	0.58